This is an *Accepted Manuscript*, which has been through the Royal Society of Chemistry peer review process and has been accepted for publication.

Accepted Manuscripts are published online shortly after acceptance, before technical editing, formatting and proof reading. Using this free service, authors can make their results available to the community, in citable form, before we publish the edited article. We will replace this *Accepted Manuscript* with the edited and formatted *Advance Article* as soon as it is available.

You can find more information about *Accepted Manuscripts* in the **Information for Authors**.

Please note that technical editing may introduce minor changes to the text and/or graphics, which may alter content. The journal's standard **Terms & Conditions** and the **Ethical guidelines** still apply. In no event shall the Royal Society of Chemistry be held responsible for any errors or omissions in this *Accepted Manuscript* or any consequences arising from the use of any information it contains.

Journal Name

ARTICLE

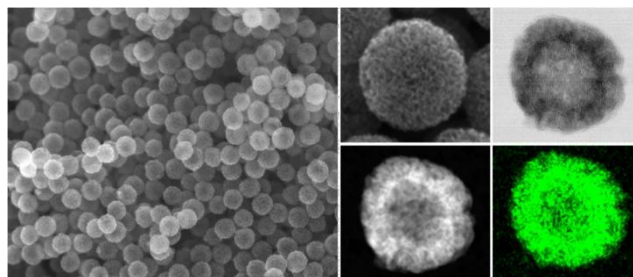# A co-sol-emulsion-gel synthesis of tunable and uniform hollow carbon nanospheres with interconnected mesoporous

JianhuaHou,[a] Tai Cao,[a] FaryalIdrees[a] and Chuanbao Cao*[a]

TOC Figure   Monodispersed tunable nanoscale hollow carbon spheres with an open interconnected mesoporous shell have been synthesized by a co-sol-emulsion-gel method.

Monodispersed mesoporous hollow spheres of polymer-silica and carbon-silica nanocomposite with an "interpenetration twins" nanostructure have been successfully synthesized by a co-sol-emulsion-gel method. The obtained mesoporous hollow carbon spheres (MHCSs) exhibited an open interconnected mesoporous shell that endows high specific surface area (S_{BET}, 2106-2225 m^2/g) and large pore volume (1.95-2.53 cm^3/g). Interestingly, the diameter of the uniform MHCSs could be precisely tuned on demand, as an effective electrode materials in supercapacitors, MHCSs with diameter of 90 nm deliver the shortest time constant (τ_0=0.75 s), which are highly beneficial for rate capacitance (180 F/g at 100 A/g, a full charge-discharge within 0.9 s) and cyclic retainability (3% loss after 20000 cycles). The new developed synthesis route leads to unique interconnected mesoporous hollow carbonaceous spheres with open-framework structures, providing a new materials platform in energy storage.

Introduction

The unique and subtle combination of hollow architectures with mesoporous nanostructures has the advantages of large void spaces[1,2] high surface area[3] and low density[4], so the design and controlled fabrication of mesoporous hollow carbon spheres (MHCSs) is very significant.[5-8] MHCSs have diverse applications in the field of adsorption[6], drug delivery[7,8], catalysis,[9,10] nano-devices,[11-15] and energy storage/conversion[16-19]. When MHCSs have interconnected open mesoporous channels within carefully controlled shell thickness and channel length, their performance was enhanced and even might open up various potential applications. [12-14]

The template methods have been well accepted as common strategies to synthesize hollow carbon nanospheres (HCSs) over the past few decades, including hard-template and soft-template method.

In general, hard-template method involves multiple steps in which the core formation of Polymer or SiO_2 nanoparticles is a key step.[6,20,21] For instance, dispersible HCSs with high uniformity are synthesized using a strict dual core-shell-type (polystyrene@phenolic resin@SiO_2) structure that polystyrene and SiO_2 are combined into a confined nanospace at high-temperature pyrolysis. [6] However, their limited surface area and porosity need to be further increased through physical post-activation treatment.[6] Furthermore, diameter (<100 nm), pore sizes and mesostructure of replicated HCSs are limited to their parental template.[7, 22] The soft-templating method usually needs fewer steps to synthesize MHCS when compared with hard-templating techniques. Whereas the obtained MHCSs are not uniform in size (normally size-variance is greater than 150 nm and not well defined), hollow core sizes and the shell thicknesses are also restricted.[6-8,23,24] Furthermore,

monodispersed nano scale MHCSs are difficult to obtain, due to their weak self-assembly with precursor components, and tendency towards cross-linking with adjacent nanospheres during pyrolysis process.[12,13,25,26] Recently, extension of the Stöber method was found effective for HCSs synthesis by removal of silica from silica/carbon nanocomposite materials.[25-28] However, it is complicated to control core/shell size, and small nanoparticles are often found as well. Moreover, resulting small pores do not possess accessible mesochannels, which hinder the potential applications.[26] Nevertheless, there is a great need to prepare high-quality MHCSs materials *i.e.* ones with highly uniform, monodispersed tunable particle size and adjustable shell thickness.[6,13] Specifically, generated well-defined MHCSs (<100 nm) with open interconnected mesoporous channels using a facile approach are still unavailable in literature.[12-13] It has stimulated substantial interests for highly effective diffusivity and ultrahigh loaded capacity for active guest molecules/ions. The reason is that the guest molecules/ions can penetrate or diffuse through hollow voids easily by means of accessible open interconnected mesochannels in shell.[5-8, 13]

Keeping all challenges in mind, herein we report a novel synthesis of hollow-structured uniform polymer-silica and carbon-silica nanocomposite spheres with tailorable nano-size and shell thickness using a simple co-sol-emulsion-gel method. The generation process of MHCSs is illustrated in Scheme 1. It is a one-pot synthesis method which uses resorcinol-formaldehyde (RF) (polymer precursor), tetraethyl orthosilicate (TEOS, inorganic precursor) and cetyltrimethyl ammonium bromide (CTAB) as template. The sol-gel rates of RF and TEOS, the formation of silica spheres is faster, which requires shorter reaction time compared to the RF spheres under the same conditions of "the Stöber method".[25, 26] Therefore, during the co-sol-gel process are first formed with CTAB micelles and RF molecules as organic phases act as a template and then TEOS is added as an inorganic precursor, finally successful synthesis of hollow nanospheres with "interpenetration twins" mesostructures. The "interpenetration twins" mesostructure of inorganic silica functions as a nanoreactor to provide a confined nanospace, which can immensely reduce structural shrinkage of the carbon precursor during high-temperature annealing. After removing silica from "interpenetration twins" (carbon-silica) nanocomposites, open interconnected mesoporous (2 ~ 20 nm) carbon spheres with tailorable particle size (90-240 nm) and well controlled hollow voids (45-105 nm) are obtained. The adopted approach is found to be facile, efficient for synthesis of well-defined hollow carbon nanospheres with interconnected mesoporous shells, which may provide a potential platform for energy storage applications. This method may reveal that not noly in the process of the controllable synthesis of high quality MHCSs to avoiding redundancy for hard-template method, *i.e.,* avoiding the first synthetic core steps but also effectively prevent the monodispersed nano scale hollow nanospheres aggregated for soft-template. It is a promising substitute to traditional methods for the preparation of novel open interconnected mesoporous with "interpenetration twins" mesostructures of HCSs.
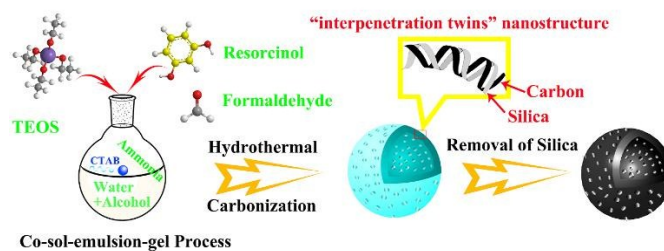
Scheme 1. The formation process of mesoporous hollow spheres of polymer-silica and carbon-silica nanocomposite with an "interpenetration twins" nanostructure by a co-sol-emulsion-gel method.

Experimental section

Synthesis ofmesoporous hollow carbon spheres (MHCSs). In a typical synthesis, resorcinol (0.2 g), and CTAB (0.6 g) were dissolved in 30 ml solution containing absolute deionized water (25~22) and ethanol (5~8 ml) at 25℃ under vigorous stirring. After resorcinol fully dissolved, ammonia aqueous solution (NH$_4$OH, 0.2 mL, 25 *wt.*%) was added and continuously stirred for 20 min, then the formaldehyde solution (0.28 mL) was added and allowed a few minutes until it changed from transparent to an emulsion, then TEOS was immediately added to the prepared solution, stirred for 24 h at 25 ℃, and subsequently heated for 24 h at 80 ℃ in a Teflon-lined autoclave. The solid product was obtained through centrifugation and freezing to dry. The obtained product was annealed at 850 ℃ for 3 h with ramp rate of 1℃/min under nitrogen flow and mesoporous hollow carbon/silica sphere (MHSs-X-C/SiO$_2$) composites were obtained as a result. The mesoporous hollow carbon spheres (MCHSs-X) were obtained when silica was removed by immersing in 15 % HF aqueous solution at room temperature for 24 h, followed by subsequent washing with deionized water. Alternatively, the mesoporous hollow silica spheres (MHSs-X-SiO$_2$) were obtained by calcination of the MHSs-X-C/SiO$_2$ composites at 650 ℃ for 5 h in air. Here X represents the spherical average diameters.

Characterization. In order to see morphology more clearly field emission scanning electron microscopy (FESEM) and transmission electron microscopy (TEM) tests were performed through Hitachi S-4800, JEOL-2100F, JEM-ARM200F, respectively. Powder X-ray diffraction (XRD) patterns from at low (10-80° in 2θ) were measured through PANalytical-X-pert diffractometer (Cu Kα radiation at 40kV and 40mA). Raman spectrum was measured at 514 nm excitation by Renishaw. Dynamic light scattering (DLS) measurements were carried out on a Malvern Zetasizer NanoZS Instrument. Axis Ultra spectrometer was used for XPS analysis. Nitrogen adsorption-desorption isotherm was measured at 77K and relative pressure p/p^0 of 3.3×10^{-7}-0.989 using Micromeritics-ASAP-2020. Prior to the measurement, samples were degassed at 300 ℃ for at least 5 h. Brunauer-Emmett-Teller (BET) and density

functional theory (DFT) tests were performed to measure specific surface area and pore size distribution.

Electrochemical measurements. Electrochemical performance of MHCSs was measured for a two electrode system with 6 M KOH as electrolyte. 85 wt.% of obtained carbon, 10 wt.% of acetylene black and 5 wt.% of PTFE binder were used for electrode preparation. Stainless steel meshes were used as current collectors for the supercapacitors, with 6 M KOH as electrolyte. The electrodes were then dried under vacuum at 120 ℃ for 8 h. Then this slurry was coated on the substrate with 8-10 mg loading per 1 cm^2 area (~0.25 mm in thickness). The details of it are summarized in Table S4 and Figure S7. A polypropylene membrane was used as the separator for the supercapacitors. Cyclic voltammetry (CV), galvanostatic charge/discharge and AC impedance spectroscopy (EIS) tests were measured through the CHI660D electrochemical workstation. Impedance spectra were measured for 0.01 Hz-10 kHz frequency range with 5 mV voltage amplitude. The cutoff charge voltage for the capacitor using 6 M KOH was set as 0-1.0 V. Specific capacitance for a single electrode was calculated using equation (1)

$$c_g = \frac{2I}{(dV/dt)m} \qquad (1)$$

Where, I (A) = discharge current, dV/dt (V/s) = slope measured through discharge curve after ohmic drop and (g) m = active material mass for single electrode. Specific energy density (E_{cell}), and specific power density (P_{cell}) for symmetrical supercapacitors were also calculated by using equation (2 & 3),

$$E_{cell} = \frac{C_g \Delta V^2}{8 \times 3.6} \qquad (2)$$

$$P_{cell} = \frac{E_{cell}}{t} \qquad (3)$$

Where, ΔV (V) = cell voltage after ohmic drop, and t (h) = discharge time.
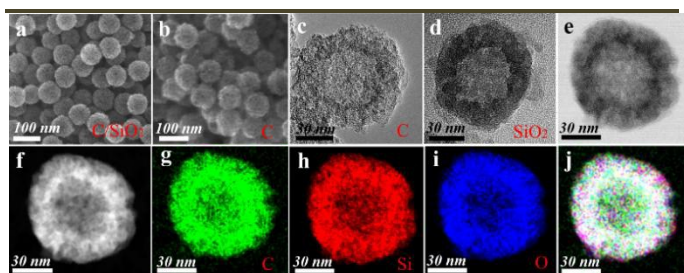
Results and discussion

Figure 1. Typical SEM images of (a) MHSs-90-C/SiO$_2$ and (b) MHCSs-90; TEM images of (c) MHCSs-90 and (d) MHSs-90-SiO$_2$; (e, f) BF and HAADF-STEM images of MHSs-90-C/SiO$_2$; (g-i) the corresponding EDX elemental mapping of carbon, silicon and oxygen, (j) along with an overlay of those three maps.

SEM images show dispersible mesoporous spheres with high uniformity and average diameter of 90 nm (Figures 1a, b). The spherical structure is well retained *i.e.*, carbon-silica composite, carbon and silica have almost the same diameter (~90 nm) and void sizes (~45 nm) (Figure 1a-d). These indicate that carbon and silica based on the "interpenetration twins" structure formation of the composites material (Figures 1a) and they also have a self-governing framework (Figure 1b-d). The high angle annular dark field and bright field scanning transmission electron microscopy (BF-STEM, HAADF-STEM) images (Figure 1e, f) and elemental mapping images (Figures 1g-j) further confirmed that "interpenetration twins" mesostructures are crossing each other in a uniform and interlocking manner. The evidence of "interpenetration twins" is further explained through magnified and wrecked images of the nanospheres in Figures (S2，S3). Their equal contribution over nanospheres are confirmed through EDX analysis (Figures 1g-j & Figure S1). These "interpenetration twins" mesostructure of inorganic silica can possibly function as a nanoreactor to provide a confined nanospace, which reduces structural shrinkage during annealing.[6] By removing one template from "interpenetration twins", these interpenetrating interfaces converted into interconnected mesoporous which endows a storage space, a large pore volume and crucial channel for active small molecules to penetrate or diffuse in hollow voids easily.
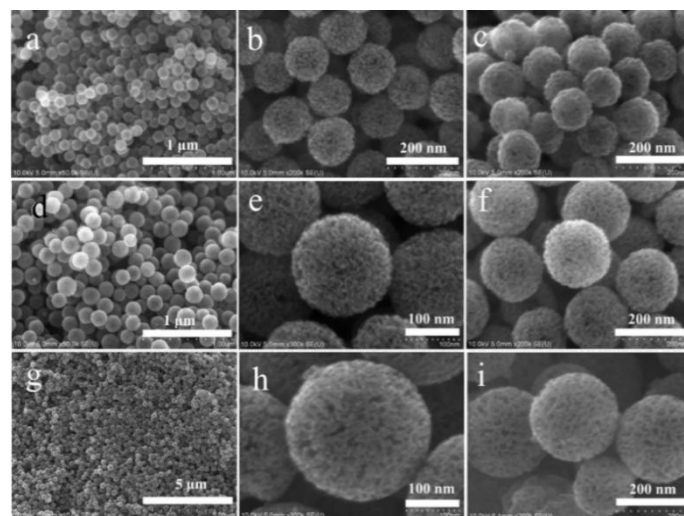

Figure 2. SEM images of MHSs with tunable sizes (a, b) MHSs-125-C/SiO$_2$, (c) MHCSs-125, (d, e) MHSs-175-C/SiO$_2$, (f) MHCSs-175, (g, h) MHSs-240-C/SiO$_2$, (i) MHCSs-240.
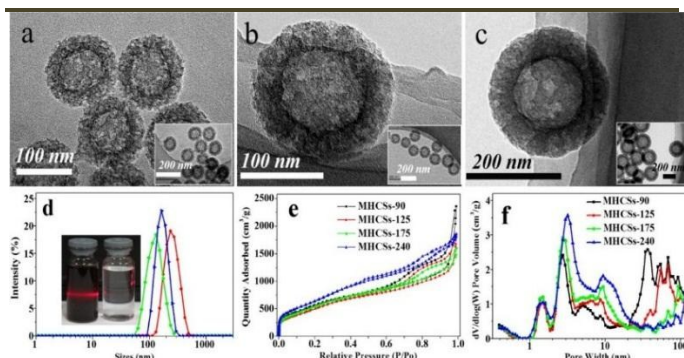
Figure 3. TEM images of (a) MHCSs-125, (b) MHCSs-175, (c) MHCSs-240, corresponding insets at different resolutions, (d) Dynamic light scattering (DLS) curves of MHCSs-125, MHCSs-175 and MHCSs-240, inset shows photograph of the dispersed solution and obvious Tyndall effect, (e) Nitrogen adsorption-desorption isotherm, and (f) Pore size distribution.

The diameters of silicon dioxide colloid spheres[29] and RF colloid spheres[30] under "Stöber method" conditions can be tailored by changing the water/ethanol volume ratio, respectively. Undre this inspiration, diameter of MHCSs also can be facilely and precisely modulated by varying water/ethanol volume ratio. For instance, SEM and TEM images (Figure 2, Figures 3a-c) show dispersible MHCSs with high uniformity and average diameters of 125, 175, and 240 nm synthesized by changing water/ethanol volume ratio from 25:5-22:8. Further, their corresponding hollow voids are 70, 97 and 105 nm, respectively. An open interconnected mesoporous (>5 nm) network structure on shells can be clearly observed through FESEM and HRTEM (Figure 2 and Figure S4). The open interconnected mesoporous shell is important for facile mass transport channels.[8, 13] Dynamic light scattering (DLS) data indicated MHCSs (MHCSs-125, MHCSs-175 and MHCSs-240) are well dispersed with particle sizes of 130, 170 and 235 nm and their polydispersity index is less than 8 % (Figure 3d). It is important to mention that we have not use any surfactant or polymer, the uniform dispersed system is stable with no sign of aggregated precipitation over one month in water or ethanol, electrostatic repulsion should be responsible for this stabilization. The nitrogen adsorption-desorption shows a type-IV isotherm (Figure 3e), clearly demonstrating the unique hierarchical mesoporous characteristics of MHCSs. The pore size distribution (Figure 3f) is calculated by using density functional theory (DFT). These multimode peaks are associated with: a) micropores (1.1-2 nm) from the phenolic resin pyrolysis, b) mesoporous (2-20 nm) by removing the surfactant and the silica from "interpenetration twins" mesostructures of as-made material, and c) meso-macroporous (20-110 nm) which may be derived from the hollow voids and/or between the carbon spheres. The above results are in good agreement with TEM and SEM. The high S_{BET} (pore volume) of MHCSs is 2106-2225 m^2/g (1.95-2.53 cm^3/g), which is higher than other HCSs.[5-7, 18-28, 31] The details of porosity properties are summarized in Table 1, S2. In addition, the shell thickness can also be tuned by simply increasing the TEOS amount

(SiO$_2$ precursor) *i.e.*, for 1.5 ml the shell thickness increases to 48 nm (*avg*) from original (39 nm) and for 2 ml it corresponds to an increase in shell thickness to 56 nm (*avg*), without any obvious change of core size of MHCSs-175 (Figure S5). Furthermore, we found that the S_{BET} slightly decreases with the increase of the hollow spherical shell, *i.e.*, from 2203 to 1965 and 1858 m^2/g, however, the pore volume increases, *i.e.*, from 1.96 to 2.46 and 2.51 cm^3/g and the average pore diameter also increases from 5.32 to 5.93 to 6.53 (Figure S6 and Table S3). This effect is possibly attributed to the increase of SiO$_2$ in the "interpenetration twins" nanostructure which can effectively fill the space of carbon materials.

These high S_{BET} and total pore volumes are due to interconnected multimode mesoporous nanostructures from an "interpenetration twins" mesostructure. Hierarchical nanostructured carbons (MHSCs) within-interconnected hollow voids/mesoporous shell have improved super-capacitance as compared with single-sized porous carbon materials because of improved mass transport, higher selectivity and increased S_{BET}.[7-11] In addition, the open accessible mesoporous channels and small size of MHSCs (especially less than 100 nm) also can be effectively used for loading, grafting, and linking functional nanoparticles/ligands for multiple therapies including drug delivery and bioimaging diagnosis.[12-14]

Table 1. Porosity properties and distribution of pore volume of typical MHCSs

Sample	S_{BET} [a]	Pore vol and (pore vol%)[b] (cm^3/g)			
	(m^2/g)	V_{total}	$V_{<2 nm}$	$V_{2-10 nm}$	$V_{>10 nm}$
MHCSs-90	2225	2.53	0.23(9.1)	0.74(29.2)	1.56(61.7)
MHCSs-125	2106	2.11	0.20(9.5)	0.94(44.5)	0.97(46.0)
MHCSs-175	2203	1.96	0.25(12.8)	1.07(54.9)	0.64(32.3)
MHCSs-240	2186	2.18	0.28(12.9)	1.30(59.6)	0.6 (27.5)

[a] Surface area is calculated with Brunauer–Emmett–Teller (BET) method by using a relative pressure range from 0.05-0.28. [b] The volume of pores smaller than 2 nm ($V_{<2 nm}$), pores between 2 and 10 nm ($V_{2-10 nm}$), and pores larger than 10 nm ($V_{>10 nm}$) obtained by DFT.

Consequently, the possible synthesis mechanism of polymer-silica and carbon-silica nanocomposites hollow spheres with "interpenetration twins" mesostructures is proposed here. Initially emulsion droplets are formed due to hydrogen bonding of CTAB micelles and numerous hydroxymethyl-substituted species (formed by a quick reaction of resorcinol and formaldehyde in water/alcohol solution with ammonia molecules as a catalyst).[32-34] The spherical diameter is limited by formation of emulsion droplets.[30] A strong electrostatic interface interaction occurs between silicate anions and surfactant molecule cations (CTAB).[35-37] Oligomer silicate species also react with the hydroxyl group of hydroxymethyl-substituted

species or resorcinol-formaldehyde (RF).[34] During the co-sol-gel process they get assembled, cross-linked and condensed such as to form an "interpenetration twins" framework.[26] While RF precursors exhibit structural similarities to silanes, *i.e.* similar coordination sites, tetrahedral geometry, three-dimensional (3D) networks nanostructures and formed spherical morphology which also undergo hydrolysis and subsequent condensation process under "the classical Stöber method"conditions.[25-31] The formation of silica spheres occurs quickly and requires shorter reaction time compared to the RF spheres under the same conditions of sol-gel process.[25, 26] Therefore, emulsion droplets are first present with CTAB micelles and hydroxymethyl-substituted species or RF through electrostatic interactions to generate CTAB-coated hydroxymethyl-substituted species hybrid aggregates as a soft template.[26] Then TEOS is added as an inorganic precursor, which can bind to the surface of emulsion droplets *via* the strong electrostatic interactions with CTAB cations (CTA^+),[26,31] avoiding the excessive cross-linking between RF micelles. It also hinder RF could diffuse into the emulsion droplets and RF polymerize with silicates, therefore hollow RF-silica nanospheres are obtained. These act as a template for each other in a homogeneous manner and finally successful synthesis of monodisperse hollow nanospheres with "interpenetration twins" mesostructures takes place.[26, 31]

By increasing the water/ethanol volume ratio, the hydroxymethyl-substituted species or RF molecules and silicate oligomers have lower bending energy and surface tension, which results a smaller emulsion droplets and eventually, and a smaller polymer-silica colloids spheres are obtained.[25,26,29-31], At the same time, with the higher water concentration, the hydrolysis rate of TEOS was increased, thus resulting in a fast nucleation and a decrease of their final diameter.[38]

XRD pattern shows two weak and broad characteristic peaks corresponding to the (002) and (101) plan (Figure S7a). Figure S7b presents the Raman spectrum of MHCSs-90 which indicates the presence of G-band at 1593 cm^{-1} (related to graphitic carbon) higher than its D-band at 1363 cm^{-1} (attributed with defects). The peak intensity ratio of G-band to D-band is around 1.15 which reflects that MHCSs-90 have relatively high graphitized contents.[39] X-ray photoelectron spectroscopy (XPS) (Figure S7c) shows C, O, and N contents in MHCSs-90 are 94.1, 4.0, and 1.28 wt%, respectively.

The MHCSs provide a hollow core with open interconnected mesoporous structure, a thin shell for ion-buffering reservoirs and facile ion diffusion channels. Therefore, they decrease the ion transport length to enhance the charge transfer rate, which are basic requirements of extensive application as high-rate energy storage devices.[40-44] For example, in supercapacitors the MHCSs have high S_{BET}, sufficient active sites and facile carriage channels for rapid mass transport, which should be beneficial for electrochemical energy storage in high-performance electrode materials.

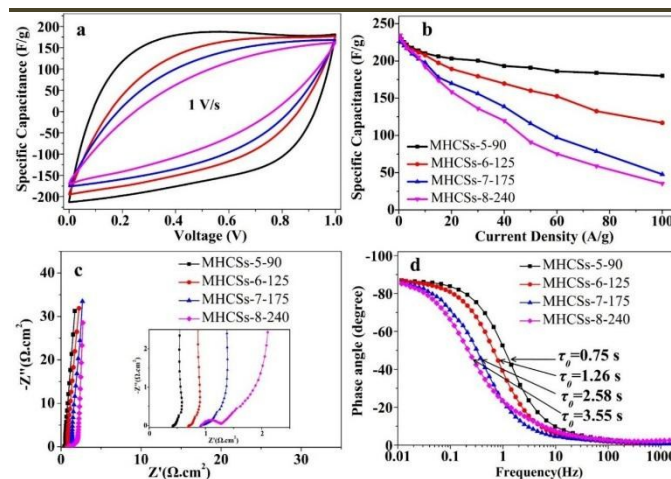**Electrochemical Characterization of Symmetric MHCSs Supercapacitors.**

Figure 4. Electrochemical characterization of MHCSs (Φ=90, 125, 175 and 240 nm, respectively) in the 6 M KOH electrolyte in a two-electrode system. (a) Cyclic voltammograms at 1 V/s; (b) Specific capacitances at different current densities; (c) Nyquist plots and (d) Bode plots of phase angle versus frequency.

The supercapacitors performances of the MHCSs were measured by a two-electrode symmetrical system in 6 M KOH. The cyclic voltammetry (CV) curves (Figure S8a) of all samples showed symmetrical rectangular shaped at 0.1 V/s, which indicate an ideal double-layer capacitance behavior.[40] With MHCSs diameter increasing, the area of CV curves gradually reduces with a highly distorted shape at relatively higher scan rate of 1 V/s (Figure 4a). This indicates that the thin shell of MHCSs delivers the advantage of short ion-transport distance. Galvanostatic charge-discharge tests were performed at various current densities (Figure 4b). By the increase of MHCSs diameter (90-240 nm), capacitances of all MHCSs are almost equal at low current density, *i.e.*, ~230 F/g at 0.5 A/g and it maintained at relative high value ~200 F/g under high current density of 10 A/g. The high electrochemical performances obtained are most likely due to large S_{BET} and interconnected hierarchical porosity for enhanced active sites, facilitate fast ion diffusion kinetics.[40] However, at a high current density of 100 A/g, Φ=90 nm of MHCSs the specific capacitances is still maintained at 180 F/g (~78% of the capacitance retention), much greater than the other *i.e.*, Φ=125, 175 and 240 nm which reveal different specific capacitances of 107, 45 and 26 F/g (~47 %, ~21 % and ~11 % of the capacitance retention), respectively (Figure 4b). The thin shell thickness of MHCSs with open interconnected mesoporous can shorten the ion-transport distance and ease the ion-transfer pathway, ultimately leading to high-rate supercapacitance. Therefore, electrochemical performances of the MHCSs-90 could be better than previously reported phenolic resin-based porous carbon [31, 41], and even superior to some advanced carbon materials for high power supercapacitors (120-160 F/g at 50 A/g [42-45]). The Nyquist plots show an almost vertical curve in the low frequency region, indicating good capacitor behavior for MHCSs (Figure 4c).[40-45] While in the high frequency region (Figure 4c inset) the 90 nm MHCSs not only have relatively lower equivalent series resistance

than others but they also show a much shorter Warburg region portion than that of 120, 175 and 240 nm MHCSs, indicating better ion diffusion efficiency.[42-46] The corresponding time constant τ_0 [47] also responded in a similar fashion (Figure 4d), *i.e.*, with 2.7 times reduction of MHCSs diameter corresponding to a τ_0 decrease by a factor of 4.7 (3.55-0.75 s). MHCSs-90's superior performances can primarily be attributed to its thin shell thicknesses and pore walls compared with others.[31] In addition, MHCSs with the diameter of 90 nm exhibited a small *IR* drop with smooth, symmetric and well-defined charge-discharge lines at a high current density (Figure S8b). They also showed high stability of 97 % after 20,000 cycles at 5 A/g compared to initial cycle (Figure S8c). Power and energy density comparison of the MHCSs-90-based supercapacitors with others advanced porous carbon materials can be seen in Figure S10 which confirm its excellent performance especially in terms of power density (>10 KW/kg). [31, 42-45]

The superior electrochemical performance is achieved through MHCSs electrodes due to multiple synergistic effect[46] of the unique material structure: (i) high S_{BET} (2106-2225 m^2/g) can provide adequate active sites for adsorbing ions, and as a result large capacitance; [41-46] (ii) hollow cores are able to form ion buffering reservoirs and offer a short diffusion path between electrode and ions to facilitate electron transfer;[31] (iii) interconnected multimode mesoporous can afford fast ion channels to accelerate ion transport which minimizes polarization effects and maximizes rate[43-46]; (iv) nanoscale spherical morphology provides high microstructure and electrochemical stability; (v)The thinner shell thickness of MHCSs own the shorter ion-transport distance and easer ion-transfer pathway, ultimately leading to higher rate supercapacitance.

Conclusion

In summary, we have designed a novel strategy for "interpenetration twins" mesostructure to synthesize dispersible and uniform mesoporous hollow spheres using a co-sol-emulsion-gel method. Remarkably, open interconnected mesoporous (2-20 nm) hollow carbon spheres with tunable particle size (90-240 nm), corresponding hollow voids (45-105 nm), high surface area (~ 2200 m^2/g) and pore volume (1.95-2.53 cm^3/g) are obtained through this technique. Furthermore, this method is favorable for its potential applications to high-rate energy storage devices. This "interpenetration twins" mesostructure design strategy can also be applied to preparation of well-defined interconnected porous hollow spheres materials, *e.g.*, silica, polymers and a wide range of nanocomposites. Our synthesized polymer, silicon dioxide and carbon spheres are important for various applications including electrode materials, photonics, adsorbents, catalyst loading and multi-drug delivery applications.

Acknowledgements

*a*Reseach Centre of Materials Science, Beijing Institute of Technology, Beijing 100081, People's Republic of China.

Corresponding Author

E-mail address: cbcao@bit.edu.cn; Tel: +86 10 6891 3792; Fax: +86 10 6891 3792.

Notes and references

1   F. Caruso, R. A. Caruso, H. Möhwald, *Science*, 1998, **6**, 1111-1114.

2   D. Walsh, S. Mann, *Nature*, 1995, **377**, 320-323.

3   A. Imhof, D. J. Pine, *Nature*, 1997, **389**, 948-951.

4   S. A. Johnson, P. J. Ollivier, T. E. Mallouk, *Science*, 1999, **12**, 963-965.

5   A. H. Lu, W. C. Li, G. P. Hao, B. Spliethoff, H. J. Bongard, B. B. Schaack, F. Schüth, *Angew. Chem. Int. Ed.*, 2010, **122**, 1659-1662.

6   A. H. Lu, T. Sun, W. C. Li, Q. Sun, F. Han, D. H. Liu, Y. Guo, *Angew. Chem. Int. Ed.*, 2011, **50**, 11765-11768.

7   Y. Fang, D. Gu, Y. Zou, Z. Wu, F. Li, R. Che, Y. Deng, B. Tu, D. Zhao, *Angew. Chem. Int. Ed.*, 2010, **49**, 7987-7991.

8   Y. Chen, P. Xu, M. Wu, Q. Meng, H. Chen, Z. Shu, J. Wang, L. Zhang, Y. Li, J. Shi, *Adv. Mater.*, 2014, **26**, 4294-4301.

9   X. Sun, Y. Li, *Angew. Chem. Int. Ed.*, 2004, **43**, 597-601.

10   S. H. Joo, S. J. Choi, I. Oh, J. Kwak, Z. Liu, O. Terasaki, R. Ryoo, *Nature*, 2001, **412**, 169-172.

11   G. Zheng, S. W. Lee, Z. Liang, H. W. Lee, K. Yan, H. Yao, H. Wang, W. Li, S. Chu, Y. Cui, *Nat. Nanotechnol.*, 2014, **9**, 618-623.

12   B. Z. Fang, J. H. Kim, M. S. Kim, J. S. Yu, *Acc. Chem. Res.*, 2013, **46**, 1397-1406.

13   Y. Li, J. Shi, *Adv. Mater.*, 2014, **26**, 3176-3205.

14   J. Liu, N. P. Wickramaratne, S. Qiao, M. Jaroniec, *Nat. Mater.*, 2015, **14**, 763-774.

15   R. Liu, S. M. Mahurin, C. Li, R. R. Unocic, J. C. Idrobo, H. Gao, S. J. Pennycook, S. Dai, *Angew. Chem. Int. Ed.*, 2011, **50**, 6799-6802.

16   G. H. Wang, J. Hilgert, F. H. Richter, F. Wang, H. J. Bongard, B. Spliethoff, C. Weidenthaler, F. Schüth, *Nat. Mater.*, 2014, **13**, 293-300.

17   B. You, J. Yang, Y. Suna, Q. Sua, *Chem. Commun.*, 2011, **47**, 12364-12366.

18   J. Liu, T. Yang, D. Wang, G. Lu, D. Zhao, S. Qiao, *Nat. Commun.*, 2014, **4**, 2798-2804.

19   A. D. Roberts, X. Li, Zhang, H. *Chem. Soc. Rev.*, 2014, **43**, 4341-4356.

20   R. J. White, K. Tauer, M. Antonietti, M. M. Titirici, *J. Am. Chem. Soc.*, 2010, **132**, 17360-17363.

21   F. Böttger-Hiller, P. Kempe, G. Cox, A. Panchenko, N. Janssen, A. Petzold, T. Hurn-Albrecht, T. L. Borchardt, M. Rose, S. Kaskel, C. Georgi, H. Lang, S. Spange, *Angew. Chem. Int. Ed.*, 2013, **52**, 6088-6091.

22   Y. Wan, H. Yang, D. Zhao, *Acc. Chem. Res.*, 2006, **39**, 423-432.

23   J. Fu, Q. Xu, J. Chen, Z. Chen, X. Huang, X. Tang, *Chem. Commun.*, 2010, **46**, 6563-6565.

24   Z. Yang, Y. Zhang, J. H. Kong,S. Y.Wong, X. Li, J. Wang, *Chem. Mater.*, 2013, **25**, 704-710.

25   A. B. Fuertes, V. V. Patricia, S. Marta, *Chem. Commun.*, 2012, **48**, 6124-6126.

26   X. Zhang, Y. Li, C. Cao, *J. Mater. Chem.*, 2012, **22**, 13918-13921.

27   X. Fang, S. Liu, J. Zang, C. Xu, M. Zheng, Q. Dong , D .Sun, N. Zheng. *Nanoscale*, **2013**, *5*, 6908-6916.

28   B. Guan, X. Wang, Y. Xiao, Y. Liu, Q. Huo. *Nanoscale*, 2013, **5**, 2469-2475.

29   W. Stöber, A. Fink, E. Bohn, *J. Colloid Interface Sci.*, **1968**, *26*, 62-69.

30   J. Liu, S. Qiao, H. Liu, J. Chen, A. Orpe, D. Zhao, G. Lu, *Angew. Chem. Int. Ed.*, 2011, **50**, 5947-5951.

31   Z. A. Qiao, B. Guo, A. J. Binder, J. Chen, G. M. Veith, S. Dai, *Nano Lett.*, 2013, **13**, 207-212.

32   D. Gu, H. Bongard, Y. Deng, D. Feng, Z. Wu, Y. Fang, J. Mao, B. Tu, F. Schüth, D. Zhao, *Adv. Mater.*, 2010, **22**, 833-837.

33   R. Liu, Y. Shi, Y. Wan, Y. Meng, F. Zhang, D. Gu, Z. Chen, B. Tu, D. Zhao, *J. Am. Chem. Soc.*, 2006, **128**, 11652-11662.

34   A. H. Lu, G. P. Hao, Q. Sun, *Angew. Chem. Int. Ed.*, 2011, **50**, 9023-9025.

35   Q. Huo, D. I. Margolese, U. Ciesla, P. Feng, T. E. Gier, P. Sieger, R. Leon, P. M. Petroff, F. Schüth, G. D. Stucky, *Nature* 1994, **368**, 317-321.

36   S. H. Tolbert, A. Firouzi, G. D. Stucky, B. F. Chmelka, *Science*, 1997, **278**, 264-268.

37   Y. Han, J. Y. Ying, *Angew. Chem. Int. Ed.*, 2005, 44, 288-292.

38   Z. Teng, S. Wang, X. Su, G. Chen, Y. Liu, Z. Luo, W. Luo, Y. Tang, H. Ju, D. Zhao, G. Lu, *Adv. Mater.* **2014**, *26*, 3741-3747.

39   C. Hu, L. Wang, Y. Zhao, M. Ye, Q. Chen, Z. Feng, L. Qu, *Nanoscale*, 2014, **6**, 8002-8009.

40   J. Hou, C. Cao, X. Ma, F. Idrees, B. Xu, X. Hao, W. Lin, *Sci. Rep.* 2014, **4**, 7260-7265.

41   X. Fang, J. Zhang, X. Wang, M. S. Zheng, N. Zheng, *J. Mater. Chem. A*, 2014, **2**, 6191-6197.

42   Y. S. Yun, S. Y. Cho, J. Shim, B. H. Kim, S. J. Chang, S. J. Baek, Y. S. Huh, Y. Tak, Y. W. Park, S. Park, H. J. Jin, *Adv. Mater.*, 2013, **25**, 1993-1998.

43   K. Xie, X. Qin, X. Wang, Y. Wang, H. Tao, Q. Wu, L. Yang, Z. Hu, *Adv. Mater.*, 2012, **24**, 347-352.

44   W. Qian, F. Sun, Y. Xu, L. Qiu, C. Liu, S. Wang, F. Yan, *Energy Environ. Sci.* 2014, **7**, 379-386.

45   B. You, J. Yang, Y. Sun, Q. Su, *Chem. Commun.*, 2011, **47**, 12364-12366.

46   J. Hou, C. Cao, F. Idrees, X. Ma, *ACS Nano*. 2015, **9**, 2556-2564.

47   X. Yang, C. Cheng, Y. Wang, L. Qiu, D. Li, *Science*, 2013, **341**, 534-537.